Design of a time-efficient video-goniophotometer combining bidirectional functions assessment for transmission and reflection

Marilyne Andersen *, Christian Roecker, Jean-Louis Scartezzini

Solar Energy and Building Physics Laboratory (LESO-PB), Swiss Federal Institute of Technology (EPFL), Building LE, 1015 Lausanne, Switzerland

Abstract

A detailed knowledge of the light distribution characteristics through advanced window systems is required to improve the visual comfort of the building's occupants while controlling the propagation of daylight in rooms and the solar gains. An innovative bidirectional goniophotometer has recently been set up for this purpose, using digital image capture and the projection of the emerging light on a diffusing screen. It therefore provides a continuous investigation of the bidirectional transmission figures in a time-efficient way. This instrument was converted into a double-purpose device, allowing both transmission and reflection measurements, which induced several strong constraints due to the conflict of incident and emerging light flux in reflection mode: on one hand the incident beam had to be restricted to the sample area only; on the other hand, as the screen obstructed the incoming light flux in some positions, a special opening in the latter was required. The practical answer to these constraints, detailed in this paper, proved to be reliable, appropriate and efficient.

Preprint submitted to Elsevier Science *1 August 2004*

Key words: Bidirectional Transmission (Reflection) Distribution Function (BTDF, BRDF), Goniophotometer, Digital imaging (CCD camera), Daylighting

1 Introduction

Advanced daylighting strategies have been developed at different levels to improve energy efficiency by minimizing both electric lighting and heating or cooling loads of buildings; at the same time, enhancing the contribution of daylight was proved to enhance greatly the visual comfort and indoors environment of the users.

This effort in optimization has lead to the development of a large variety of innovative fenestration systems [1, 2, 3, 4], including solar blinds, novel glazing or coating materials and daylight-redirecting devices, whose directional properties need to be assessed accurately to allow their efficient integration in buildings and to benefit from their potential as energy-efficient strategies. The quantity used to describe these properties, angle-dependent at both the incidence and the emerging levels, is called Bidirectional Transmission (or Reflection) Distribution Function, abbreviated BTDF (or BRDF). This function is defined as the quotient of the luminance of a surface element in a given direction by the illuminance incident on the material [5], and hence expresses the emerging light distribution for a given incident direction.

* Corresponding author. Present address: Building Technology Program, Department of Architecture, Massachusetts Institute of Technology, Building 5-418, 77 Massachusetts Avenue, Cambridge, MA 02139-4307, USA. Tel: +1-617-253-7714; fax: +1-617-253-6152.

Email address: mand@mit.edu (Marilyne Andersen).

URL: http://architecture.mit.edu/people/profiles/prander.html (Marilyne Andersen).

The use of video techniques, together with digital image handling software, has proven to be a very fruitful and encouraging approach in the field of photometry, especially since the advent of Charge-Coupled Device (CCD) image sensors [6], allowing considerable improvements in speed and flexibility. Already widely used for assessing luminance distributions on surfaces and reflectance properties of objects at very different scales [7, 8, 9, 10, 11, 12, 13], they allow to reduce the scanning process and achieve high spatial accuracy in the results. Several video-photometers or mapping luminancemeters were designed [14, 15, 16, 17, 18, 19], as well as CCD camera-based instruments for the modeling of lighting conditions in a given environment [20] or for road lighting assessment [21]. The sky luminance scanner described in [22] uses the reflection of the sky vault on a spherical mirror before being captured by a calibrated CCD camera.

More recent works confirmed the adequacy of this technique for the assessment of the luminous performance of buildings [23]; a more specific application was ergonomic evaluation, achieved through the use of a black and white CCD camera as a visual comfort meter [24, 25], or a color digital camera [26, 27].

One of the greatest advantages of using digital imaging techniques for photometric measurements is to allow the visualization of many directions or locations at the same time. It has been used so far mostly to investigate details on materials. However, the projection of the light emerging from the sample on a surface more easily captured by the camera would allow to prevent the latter from having to move from one acquisition position to the next one.

Two examples of instruments using digital imaging combined to this projec-

tion principle were designed for photo-realistic rendering of lighting in interior spaces, allowing to lower the processing time needed to perform a full BRDF measurement in a remarkable way In [28], a mirrored hemisphere is used as the projection surface and a fish-eye lens for the image capture; in [29], a cube coated with a diffuse grey paint replaces the mirror and thus avoids polarization effects but instead induces parasitic inter-reflections that are difficult to assess and control.

A goniophotometer based on digital imaging techniques and developed more specifically to assess advanced fenestration systems was developed for transmission measurements (BTDF) [30]. It uses a CCD camera combined to a projection screen, flat and diffusing to avoid the two undesirable effects mentioned above. The chosen approach led to an extremely satisfactory accuracy in the achieved BTDF values [31, 32] and showed an appreciable flexibility in image processing [33, 34]. It was therefore redesigned to allow reflection measurements (BRDF) as well.

The design process of the instrument combining BTDF and BRDF measurements is presented here. The two major additional constraints were that the incident beam needs to penetrate a light-proof structure in a controlled way to prevent parasitic reflections around the sample, and that several configurations will induce the projection screen itself to obstruct the beam's path. The mechanical components specifically developed to answer these constraints in a practical and efficient way are described in this paper.

2 Assessment principle

The assessment principle of this instrument is illustrated in Figure 1 and based on the reflection of the emerging light flux on a triangular diffusing screen, towards which a CCD camera is pointed [30, 35]. The camera is used as a multiple-points luminance-meter and calibrated accordingly. A luminance mapping of the projection screen is carried out by capturing images of it at different integration intervals, thus avoiding over and under-exposure effects, and appropriately combining the latter to extract BT(R)DF data at a pixel level resolution [34]. Within six 60° movements of the screen and camera system, a complete and continuous investigation of the emerging light distribution is achieved.

The light source remaining fixed, the incident direction (θ_1,ϕ_1) is determined by inclining the sample plane around a horizontal axis, and by rotating the sample around its normal.

Fig. 1. Detection of the transmitted light flux for the LESO-PB / EPFL video-goniophotometer.

3 Design of a transmission / reflection device

As far as possible, the functioning principle on which bidirectional transmission measurements are based is to be maintained for BRDF assessment, including a detection system consisting of a flat diffusing screen towards which a calibrated CCD camera is aiming and the fixed light source.

A practical and rapid conversion from one mode to the other is necessary. At

the same time, the range of possible incident directions is to remain consistent with international standards for bidirectional measurements and therefore not be too restrictive as far as angular couples (θ_1, ϕ_1) are concerned. Finally, sample illuminated areas must be appropriate for fenestration systems characterization, i.e. of about 10 cm diameter or more.

To achieve reflection measurements while keeping this particular light detection principle, the incident beam penetration into the measurement space must be carefully controlled, as incoming and emerging light are now on the same side of the sample. As illustrated on Figure 2, the illuminated surface must be restricted to the characterized sample area to minimize parasitic light detection; in addition to this, openings in the screen are required to leave the path of the incident beam free, that have to be minimized because they create blind regions where reflected light cannot be analyzed.

Fig. 2. Schematic representation of the constraints imposed for bidirectional reflection measurements.

The final concept is illustrated by the sequence of images given in in Figure 3. To control the incident light beam penetration, a synthetic strip presenting one circular hole unrolls on a quarter-circular metal sheet, fixed on the main platform. This sheet is perforated with a set of elliptic openings of dimensions given by the apparent sample surface (accounting for tilt angle θ_1) and of corresponding positions on the quarter circle arc. It serves as well as a gliding support for the motorized strip as for the final "shaping" of the beam

impinging on the sample surface.

The projection screen concept relies on the removal of elliptic covers by a robotic mechanism, described in more details in Section 5.2. The ellipses' dimensions were again determined by the apparent sample area accounting for angle θ_1, yet this time projected on a surface oblique to the sample plane with a tilt angle $\Theta_0 = \arctan\frac{2}{\sqrt{3}} \cong 49.1°$. The induced blind spot can therefore be reduced to the light beam's area exactly, which allows a minimal loss of information on the emerging light distribution. Of course, a blind spot only appears for one of the six screen positions, except for normal incidence where the tip needs to be removed for all of them.

Fig. 3. Control of incident beam penetration and path through obstructing screen.

As an overlap of two successive light beam openings was to be ruled out for the metal sheet as well as for the projection screen, the sample size had to be limited. As a matter of fact, the optimal combination of altitude step $\Delta\theta_1$ and sample diameter D are determined by both the device's geometry itself and the minimal illuminated area required to characterize fenestration systems or coating materials. Obviously, as a larger diameter D calls for a coarser resolution in θ_1, a compromise was necessary.

The distance from the ellipse at normal incidence ($\theta_1 = 0°$) and the next one ($\theta_1 = \Delta\theta_1$) on the projection screen (closer to the sample than the metal sheet) being the most critical, it is the one chosen for determining the minimal step in altitude $\Delta\theta_1$ and the maximal diameter D for reflection measurements. In this case, their relation can be deduced from trigonometric considerations,

leading to Equation (1) where $d_\perp$ is the minimal distance between the sample center and the screen plane:

$$D = 2d_\perp \cdot \frac{\tan\Theta_0 - \tan(\Theta_0 - \Delta\theta_1)}{\frac{1}{\cos\Theta_0} + \frac{1}{\cos(\Theta_0 - \Delta\theta_1)}} \tag{1}$$

Considering different intervals $\Delta\theta_1$ (1°, 5°, 10°, 12°, 15°, etc.) and calculating the corresponding values for D, it appeared that to allow sample diameters of at least 10 cm, the step in altitude had to be greater than 6° to ensure a (minimal) 1 cm margin around the theoretical elliptic shape. For practical applications, the more standard step in θ_1 of 10° was chosen, associated to a 15 cm diameter for the sample. It was verified that for such conditions, the first elliptic cover after the tip ($\theta_1 = 10°$) would be entirely comprised inside the physical screen (the panel would consist of totally separate pieces for a larger one).

Once the applicability of the design was verified, the new components were designed and constructed.

4 Light source

The main factors influencing the choice of the new source were of three kinds:

- a high illuminance uniformity over the sample area had to be reached;
- the blurredness around the sample (due to the impinging beam's control by elliptic apertures and thus responsible for parasitic reflections) had to be minimized, i.e. the region within which illuminance values grow from zero to the value at which a sufficient uniformity is achieved: to quantify blurredness, the relative difference between uniform area and full spot size

was used, the full spot being delimited by the group of all pixels brighter than the minimal greyscale level for which they are still adjacent;

- the sample illuminance had to be maximized in order to increase the signal to noise ratio.

The illuminance reached on the sample plane has a direct impact on two parameters: on one hand, it affects the relative error on the lowest detectable screen luminance (limited by the calibration instrument itself); on the other hand, it determines the threshold of observable BT(R)DF values. At the same time, it is itself determined by the source intensity and by its distance to the sample, primarily responsible for the blurred region around the sample.

To proceed to an optimal choice of the light source, an in-depth study of the relation between the beam properties and the required accuracy for the quantities implicated in a BT(R)DF assessment was achieved. Several types of light sources placed at various distances from the sample were thus analyzed and their performances assessed against these different criteria.

The stage followspot of model "Korrigan 1011+" (HMI 1.2 kW, 5/9° zoom) illustrated in Figure 4(a) fulfilled the expectations in a satisfactory way. The optimal distance, lens aperture and iris opening were determined by an extensive study of the blurredness and illuminance level variations [35]. This study led to the following settings: distance 10.3 m, lens aperture 6°10', fully open iris, 100% dimmer.

Fig. 4. Light source HMI 1.2 kW chosen for the BT&RDF goniophotometer.

The incident light spectrum is given in Figure 4(b). The achieved illuminance uniformity over the sample area was checked by moving an illuminance meter over the concerned region and normalizing the data with simultaneous measurements performed with second sensor, that was fixed. Average variations of 1.4% were observed in relative terms; they remained below 2% for grazing angles. As far as light beam collimation is concerned, its important influence on BT(R)DF values asked for a detailed analysis, presented in [35] and showing a spread that remained below 0.5°.

During a BT(R)DF characterization, the sample illuminance $E_1(\theta_1)$ is measured by ensuring an optimal simultaneity between image exposure period (integration interval) and sampling of illuminance data (averaged into a single value), also allowing to account for the slight temporal light source fluctuations, lower than 1%. This is achieved thanks to an external luxmeter (LMT, Pocket-Lux 2B, illuminance range from 0 to 20,000 lux, converted in a voltage from 0 to 10 V), connected to a data acquisition card (NI-DAQ, PCI 1200) and mounted on a static vertical rod fixed on the goniophotometer's structure, as shown on Figure 5.

Fig. 5. Independent luxmeter support for simultaneous illuminance measurement.

To establish the relation between the illuminance measured at the theoretical (sample centre) and practical (luxmeter support) locations, a second calibrated LMT luxmeter was positioned right at the sample centre; illuminance values for varying θ_1 angles were then measured with both instruments simul-

taneously. Their ratio determined the appropriate correction factor, equal to $0.81 \cos \theta_1$.

Through this experiment, the luxmeter's accuracy was verified by comparing the experimentally assessed variation of $E_1(\theta_1)$ to the (ideal) cosine law. The agreement between the two was found to be excellent (average relative difference lower than 1%).

4.1 Measurement space envelope

The measurement space envelope for combined BTDF and BRDF measurements, shown on Figure 6(a), consists of a carbon fiber cap strengthened by a structural metallic frame, shown on Figure 6(b) and made of black stainless-steel tubes presenting a 4×4 cm square section with a curved rail of 154 cm radius; this frame also supports a static stainless-steel perforated sheet on which a moving synthetic strip can glide. The latter's unique aperture is circular, slightly larger than the largest ellipse cut-out from the metal sheet (i.e. the one associated to normal incidence); the chosen 10° step in altitude ensures that a 15 cm diameter hole never overlaps two consecutive entrances. The incident beam is hence controlled through the appropriate ellipse, selected by unrolling the synthetic strip to position its circular aperture adequately (according to altitude θ_1). At the same time, light is prevented from entering the measurement space through any other opening.

Fig. 6. Structural components of the BT&RDF goniophotometer.

To automate the positioning of this circular aperture, the strip's gliding movements on its metal sheet support are driven by a motorized winder at one end (Figure 7(a)), combined to a spring system at the other (Figure 7(b)), both fixed to the support frame outside the incident beam path. An opto-sensor home switch detects the hole position in the strip (Figure 7(a)) and ensures proper positioning of the aperture.

Fig. 7. Motorized unrolling of the synthetic strip for its adequate positioning on the metal sheet.

The determination of the actual position and dimensions of the ellipses cut out from the metal sheet required a multiple stages process for an optimal incident light control:

- First, the theoretical geometric properties of the ellipses were determined based on trigonometric considerations, assuming a perfectly parallel beam reaching an elliptic surface of apparent horizontal axis 15 cm and vertical axis $15 \cdot \cos\theta_1$.
- Then, the ellipses dimensions were adjusted to the real incident beam, of imperfect collimation and thus producing blurred regions around the uniformly illuminated area, responsible for parasitic reflections. Once the optimal source distance was determined, different elliptic shapes were tried out to compare the achieved sample surface illumination. The most efficient compromise was established between optimal uniformity over the whole sample area and lower parasitic light flux; this was done for each ellipse individually, as more relative blurredness appeared for smaller ellipses. The

determined shapes, cut out of cardboard sheets, were tested successfully; they led to only few percent of non-uniformly illuminated sample area while guaranteeing an average relative blurredness area lower than 10%. It can be noted that these remaining parasitic reflections were reduced to a negligible level by adding a ring of highly absorbing material ("velvetine") around the sample.

- Finally, the positions of the ellipses on the metal sheet had to account for the frame manufacturing imperfections (see above). The metal sheet was thus mounted temporarily on the frame, allowing to centre the ellipses thanks to a plumbline course driven by a progressive platform inclination. Their positioning was thereafter verified by pointing a fixed laser on the central axis and tilting the device to get each ellipse's centre coincident with the laser spot; this test showed that an appropriate accuracy was achieved ($\pm$ 0.05 cm deviation). Before sending the metal sheet for cutting out, these positions were adjusted to a flat configuration of the sheet (i.e. to its neutral fiber), to avoid slight shifts due to the sheet's thickness.

The resulting perforated metal sheet is shown on Figure 6(b); its inside surface is covered with "velvetine" (reflection factor lower than 1%).

4.2 Main platform and sample holder

As the ceiling of the dark chamber is not high enough to allow the new source to be positioned at the proper distance (10.3 m) above the sample, it was set up on a large tripod on the floor (see Figure 4(a)), at the goniophotometer's horizontal rotation axis height.

The movements of the main platform were adapted accordingly: they were shifted 90° and adjusted to a 180° rotation from one vertical to the other. On the other hand, the camera's wiring system exit had to be redesigned to prevent any disturbance of incoming (and emerging) light for all possible tilt angles and screen positions.

The additional weight caused by the support frame and the synthetic strip system requested a mechanical compensation of the strong imbalance sustained by the main platform rotation axle. Counterweights were designed for that purpose, that compensate the torque created by the different massive elements. However, as the exact alignment of all components is crucial for the the incident beam control, the remaining slight weight effect on the main platform positioning asked for a software compensation for optimal adjustment; the correction factors (lower than 0.3°) were determined experimentally using a protractor and a spirit level; they were thereafter checked by observing the light beam centering on the sample surface.

The sample fixation system consists of a thin circular diaphragm (of varying opening size and used to restrict the illuminated sample area) sandwiched between the sample and a rigid mounting ring with four protruding parts, each one presenting two holes to screw the sample tight (see Figure 5). It had to be adapted to reflection measurements too, where the characterized surface is on the other side of the diaphragm. Therefore, special clipping elements were designed for the sample holder's ring, tightened on the four aforementioned pairs of screw holes. As far as the sample's rotation is concerned, it must be executed in opposite directions whether in transmission or reflection mode, as the referential is inverted.

This design aligns the sample illuminated plane on the main platform rotation axis for both transmission and reflection measurements and offers flexibility for the sample framing (the maximal sample size that can be handled is 40×40 cm^2). Also, it allows the limit altitude $\theta_{2_{\text{lim}}}$ at which a measurement is still reliable to reach 85° for most sample configurations.

5 Light detection system

The function of the triangular projection screen is to allow the CCD camera to view the distribution of light emerging from the characterized sample in one of the six hemisphere portions on a single image (each represents a solid angle of $\frac{2\pi}{6}$ steradian). A perfectly flat projection screen was chosen to avoid inter-reflections from one screen point to another, that would not be prevented with a hemisphere (although the latter might have appeared a more natural alternative for symmetry reasons). On the other hand, a diffusing coating is required for two reasons: to avoid polarization effects and to allow light reflected by any part of the screen to be observable likewise by the camera, without any correlation between the camera's position and the measurements.

As illustrated in Figure 8, the screen is fixed on the rotating ring opposite to the camera at an inclination angle Θ_0 from the ring plane equal to $\arctan \frac{2}{\sqrt{3}} \cong 49.1°$ by the way of adjustable carbon fiber rods; its orthogonal projection on the sample plane thus determines an equilateral triangle. As mentioned above, it had to be reconfigured to allow elliptic covers to be removed, as detailed in Section 5.2.

Fig. 8. Screen and camera facing each other on the rotating ring.

5.1 CCD video camera

The video camera based on a Charge-Coupled Device (CCD) detector (Kappa CF 8/1 DXCair, 752 x 582 pixels, with Peltier cooling system) is computer-controlled through an ad hoc digital image acquisition and handling software (Image-Pro Plus® [1]). The latter offers integration intervals comprised between 100μs and several hours, a customized adjustment of the signal converter (see [36]) and a choice between two gamma values [37]: 1 (linear response) and 0.45 (the response is a 2.2 power function), the latter value for gamma being chosen for resolution optimization reasons [30, 35].

The camera's optical system is made of a wide-angle lens (6 mm / 1.2, type H0612FI) fixed on a C-mount. The focal length cannot be varied, but the diaphragm aperture can be set manually. Using a variable polarizer to assess the camera's response to the state of polarization showed only a slight sensitivity (pixels greyscale levels only affected by 2% in relative terms), which strengthens the hypothesis that BT(R)DFs are undisturbed by polarization effects.

A special mounting support was designed for the camera and fixed on the rotating ring; to allow a full view of the screen, the camera was inclined 23° regarding the sample plane, as shown on Figure 8. A square buffer was placed in front of the camera: it prevents rays entering through the sample aperture from reaching the camera directly and producing glare effects. It was thus

[1] Image-Pro Plus® The Proven Solution™, v. 4.1.1.2, Media Cybernetics, L.P.

positioned in order to limit the camera's view exactly at the detection area's base.

The different calibration procedures necessary to convert this CCD camera into a reliable multiple-points luminance-meter are explained in details in [30, 35]. The additional corrections required to ensure a stable response of the video system and avoid any sensitivity to the room temperature are described in [36].

5.2 Diffusing projection screen

5.2.1 Geometry and material

The projection screen is an isosceles triangle of dimensions 117.7 cm (base) and 155.6 cm (perpendicular height). It is slightly larger than the effective detection area, which presents a 115 cm base (= equilateral triangle's edges) and a 152.1 cm perpendicular height, so that the difference in level H between the detection area base and its apex is equal to $152.1 \times \sin\Theta_0 = 115$ cm as well.

To allow a motorized system to installed on the screen for the elliptic covers' removal, the screen's lateral parts were made of a 1 cm thick core in PVC foam (manufactured by Alcan Airex AG), sandwiched between two 0.1 cm aluminium foils. In a 22.4 cm wide band on the central axis, where the elliptic holes are cut out, aluminium was chosen as the core material, to allow for accurate mechanical processing. This rigid support hosts the various inserts needed for the robotic system and the covers positioning. The covers themselves consist of a 1 cm thick core of Uniform® (POM) (manufactured by

BASF Plastics), sandwiched between two 0.1 cm aluminium layers.

To hold the screen in a stable tilted position (of tilt angle $\Theta_0 = 49.1°$) in reflection mode, the pair of carbon fiber rods shown on Figure 8 could not be kept as they were. Even if fixed elsewhere on the screen edges, preliminary tests revealed that there was always a configuration where they were in the incident beam's path. Therefore, a special fixing piece of hexagonal shape was designed, shown on Figure 9(a), one of its edges being modified for an apex to be added (see Figure 9(b)) to ensure an open sight of the whole screen area from the camera's point of view.

Fig. 9. Hexagonal screen fixing piece to ensure incident beam path, with added apex to avoid screen image obstruction.

Three light-emitting diodes (LED's) were added around the screen to ensure a fine (pixel level) localization of the screen detection area on the images [35]. Their respective positions were chosen as close as possible to its three summits for better accuracy; constraints due to the incident beam path had yet to be accounted for, particularly critical around the normal and next to normal (10°) incident directions. They were placed slightly backwards from the screen surface to prevent parasitic reflections, at an illumination level just sufficient to allow their precise pinpointing on the digital image. They are represented on Figure 10.

Fig. 10. Adjustment of the image pixels corresponding to the screen detection area thanks to three LED's localized on the image.

5.2.2 Coating characteristics

The screen is covered with a diffusing white paint (LMT Photometer paint PHP 80), made of a mixture of barium sulphate ($BaSO_4$) and of water-soluble binder; a selected black pigment is added to achieve a spectrally neutral reflectance over the visible range, presenting variations lower than 1.5% [30]. A Minolta CR-200b surface chromameter was used to measure the normal/diffuse reflection factor at different places on the screen: it led to a mean value of 0.749, with relative fluctuations of only 0.2%.

Thereafter, luminance values on the screen surface were measured at different emerging angular directions and for several impinging angles α to compare them with a Lambertian model (perfect diffusion); the observed average and maximal relative discrepancies for usual angles were of 2.6% and 10.6% respectively [30].

To confirm these observations, a second experiment allowing to assess the screen coating diffusion quality was realized, keeping the luminance-meter at a fixed position and varying the impinging angle α. As the illuminance of the screen decreases according to a cosine law for an increasing α angle, the luminance re-emitted towards the luminance-meter is expected to undergo the same effect if the surface is Lambertian. The results are reported on Figure 11 and show relative discrepancies lower than 1% between the observed and predicted values.

Fig. 11. Luminance on the screen surface as a function of impinging angle α compared to the expected $\cos\alpha$ law.

Furthermore, achieving a high diffusion quality allows to avoid problems caused by the sensitivity of the detection device to the polarization state, pointed out by [38] for goniophotometric measurements: as the light emerging from the sample undergoes a diffuse reflection on the projection screen, it is depolarized before reaching the CCD camera [39].

5.2.3 Elliptic covers removal

The removal of the screen covers, necessary to perform BRDF measurements, aims at leaving the incident beam path free, while the controlling of its shape is taken care of by the ellipses cut out from the metal sheet.

To minimize the blind zones, these screen covers must present elliptic shapes as well. Their exact geometry was determined following a similar procedure as for the metal sheet:

- First, their theoretical dimensions and positions were deduced by trigonometry on the basis of the intersection of a perfectly parallel beam (reaching the sample at different θ_1 angles) with the tilted detection surface (accounting for the shift between sample and detection screen base planes.
- Then, using on the results provided by the sample illumination analysis with the actual light source and on the metal sheet ellipses dimensions, adjusted horizontal and vertical axes for the screen ellipses were estimated, to which a 2 mm margin was added to avoid edge effects.
- After that, to determine the actual dimensions of the cut out covers, the thickness of the screen had to be taken into account; on the other hand, the covers insertion required a slant between the upper (external) and lower (internal) sides of the screen, chosen unique and equal to 20° to ease the

screen manufacturing. To leave the beam's passage free through a screen of significant thickness, larger upper ellipses are required when the angle between the incoming beam and the screen plane increases (i.e. when $\mid \theta_1 - \Theta_0 \mid$ increases). The ellipses were thus adjusted accordingly, depending on each one's incident tilt angle.

- Finally, as the above adjustment was only necessary for the ellipses half farthest from the $\theta_1 = \Theta_0$ direction, their vertical axes (and thus the blind zones) were reduced by re-centering them to open a passage for the actual beam only, still accounting for the screen thickness and a constant 20° slant.

The elliptic covers are held in place by small and strong permanent magnets inserted in the screen central piece. To achieve their removal and repositioning, a "permanent electro-magnet" (PEM) is used, i.e. a permanent magnet that can be deactivated by powering the surrounding coil. This PEM is mounted on a small wagon running on two rails parallel to the main axis of the screen thanks to an indented belt forming a closed loop. An additional on-board mechanism allows it to move up and down from approximately 3 cm, in order to extract and replace the covers. To ensure a reliable lifting, a mechanical "extractor" was added, using four screw-like pins that get inserted in four slots carved in each cover, shown on Figure 12(a); centering pins were added as well on protruding fingers to ensure a reliable positioning. An extra shift was implemented for the wagon movements to allow the extraction system to have a secure grip on the covers.

The limitations in the rails length made it impossible for this extractor to reach the tip cover. Its handling thus required an additional PEM device, together with some extra commands.

Fig. 12. Motorized screen with removable covers for incident beam path.

The wagon is driven by a stepping motor, controlled by a specific ISEL micro-controller with a RS-232 interface. A typical cycle of extraction, removal and replacement of a cover is sequenced as follows:

- Wagon moved above the appropriate cover, PEM deactivated and lowered, then activated again to retrieve the cover by lifting it up;
- Wagon positioned out of the beam path and kept in place as long as needed to complete the image acquisition and processing phase;
- Wagon moved back above the open hole, PEM lowered, deactivated then lifted up empty, the cover being back in place.

Once the wagon movements were adequately calibrated to position it right above each cover, this new design was tested successfully with hundreds of random extractions at different screen inclinations.

The definitive screen panel is shown on Figure 12(b), where the wagon is in position to remove the tip cover and where all other covers are missing. Figures 12(c) to 12(f) illustrate the sequence of events taking place when the projection screen obstructs the incident beam path.

6 BRDF results and validation

As detailed in [33], three types of graphical representations were developed to provide various visualization possibilities of the transmitted or reflected light distribution features, in addition to a recombined view of the six calibrated

images, gathering the latter into a unique orthogonal projection:

- the projection of the BT(R)DF values on a virtual hemisphere, allowing a precise analysis of the angular distribution;
- a photometric solid, representing the BT(R)DF data in spherical coordinates with growing radii and lighter colors for higher values, illustrated in Figure 13;
- several section views of this solid, providing an accurate display of the numerical values distribution.

Fig. 13. BRDF representation as a photometric solid.

An in-depth validation of both BTDF and BRDF was conducted, based on different approaches [35]:

- assessment of error at each intermediate stage of calibration and processing, a final error being deduced;
- bidirectional measurements of systems presenting a known symmetry and verification against standard luminance-meter data or analytical calculations;
- empirical validation based on bidirectional measurements comparisons between different devices;
- assessment of hemispherical optical properties by integrating BT(R)DF data over the whole hemisphere and comparison to Ulbricht sphere measurements [40];
- comparison of monitored data with ray-tracing simulations to achieve a higher level of details in the BT(R)DF behaviour assessment.

These studies led to a relative error on BT(R)DF data of only 10%, allowing to confirm the high accuracy and reliability of this novel device.

7 Conclusion

This paper presents the conception and construction of an innovative, time-efficient bidirectional goniophotometer based on digital imaging techniques and combining BTDF and BRDF assessments. To allow reflection measurements, a controlled passage of the incident beam into the measurement space was created, minimizing parasitic reflections around the sample. Openings in the detection screen for the situations where it obstructs the incoming light flux were also required, made as small as possible to restrict the produced blind zones; to remove these elliptic covers, a motorized extraction and repositioning system was developed and tested successfully.

This design proved efficient and reliable, for both the light beam penetration into the measurement space and the passage through the obstructing screen. The high accuracy achieved for BTDF assessments was checked to be kept for BRDF measurements as well, placing reliance on the assumptions made in the construction of the instrument.

This instrument will help manufacturers of advanced fenestration systems to develop and optimize their products, and provide guidelines to architects in their judicious selection already at the project's level. Such a detailed characterization is also necessary for daylighting simulation programs to improve their performances and achieve a reliable modeling of light propagation in rooms using advanced fenestration systems.

Acknowledgements

This work was supported by the Swiss Federal Institute of Technology (EPFL) and the Commission for Technology and Innovation (CTI). The authors wish to thank Pierre Loesch and Serge Bringolf for their contribution in the goniophotometer's mechanical development.

References

[1] I.R. Edmonds. Performance of laser-cut deflecting panels in daylighting. *Solar Energy Materials and Solar Cells*, 29:1–26, 1993.

[2] C.B. Greenberg. Optically switchable thin films: a review. *Thin Solid Films*, 251(2):81–93, November 1994.

[3] G. Courret. *Systèmes anidoliques d'éclairage naturel*. PhD thesis, EPFL, Lausanne, 1999.

[4] M. Kischkoweit-Lopin. An overview of daylighting systems. *Solar Energy*, 73(2):7782, 2002.

[5] Commission Internationale de l'Eclairage. Radiometric and photometric characteristics of materials and their measurement. *CIE*, 38(TC-2.3), 1977.

[6] S. Ochi and T. Lizuka. Charged-Coupled Device Technology. *Japanese Technology Reviews*, 30(A), 1996.

[7] K.F. Karner, H. Mayer, and M. Gervautz. An Image based Measurement System for Anisotropic Reflection. *Computer Graphics Forum*, 15(3):119–128, September 1996.

[8] I. Ashdown and R. Rykowski. Making Near-Field Photometry Practical. *Journal of the Illuminating Engineering Society*, 27(1):67–79, 1998.

[9] I. Lewin and J. O'Farrell. Luminaire Photometry Using Video Camera. *Journal of the Illuminating Engineering Society*, 28(1):57–63, 1999.

[10] S.R. Marschner, S.H. Westin, E.P.F. Lafortune, K.E. Torrance, and D.P. Greenberg. Image-based BRDF measurement including human skin. In *Proceedings Eurographics Workshop on Rendering*, Granada, Spain, June 21-23, 1999.

[11] D.R. Jenkins and H. Mönch. Source Imaging Goniometer Method of Light Source Characterization for Accurate Projection System Design. In *2000 Society for Information Display Conference*, Long Beach, CA, 2000. SID.

[12] A. Demircan, R. Schuster, M. Radke, M. Schnermark, and H.P. Rser. Use of a wide angle CCD line camera for BRDF measurements. *Infrared Physics & Technology*, 41(1):11–19, February 2000.

[13] H.P.A. Lensch, J. Kautz, and M. Goesele. Image-Based Reconstruction of Spatial Appearance and Geometric Detail. *ACM Transactions on Graphics*, 22(2):234–257, April 2003.

[14] M.S. Rea and I.G. Jeffrey. A new luminance and image analysis syste, for lighting and vision - I. Equipment and calibration. *Journal of the Illuminating Engineering Society*, 19(1):64–72, 1990.

[15] I. Lewin, R. Laird, and J. Young. Video photometry for quality control - CCD technology produces an all-terrain photometer system. LD&A, pp. 16-20, January 1992.

[16] K.D. Song, L.O. Degelman, and L.L. Boyer. Determining Daylighting Parameters by a Luminance Mapping System and Scale Models. *Journal of the Illuminating Engineering Society*, 23(1):65–75, 1994.

[17] I.C. Pasini and B.W. Transley. Assessing the Luminous Environment with IQ CAM SCENE Video Photometer/Colorimeter. In *Light Wave, IESNA Conference*, 1994.

[18] V. Berrutto. *Métrologie de la qualité visuelle des ambiances lumineuses: Application à l'éclairage des bureaux*. PhD thesis, Université de Savoie, Chambéry, 1996.

[19] B.W. Tansley, K.W. Houser, and I.C. Pasini. The IQCam Digital Image Photometer System: Principles of Operation and Comparative Performance. *Journal of the Illuminating Engineering Society*, 28(1):182–200, 1999.

[20] C. Loscos. *Ré-éclairage et Remodélisation Interactifs des Scènes Réelles pour la Réalité augmentée*. PhD thesis, Université Grenoble I, Grenoble, December 1999.

[21] J. Glenn, G. Dodds, and R. Robinson. Practical limitations and measurements for camera based road luminance / lighting standards assessment. *Journal of the Illuminating Engineering Society*, 28(1):64–70, 1999.

[22] L. Michel and M. Andersen. Réalisation d'un photo-uranotomographe à imagerie numérique. In *Proceedings Solar Energy in Buildings CISBAT'99*, pages 289–294, Lausanne, Sept. 22-23, 1999. EPFL.

[23] C. Dittmar, H. Schuster, M. Oetzel, and H. Müller. Validation process of daylighting test facilities at the University of Dortmund. In *Proceedings CISBAT 2003*, pages 235–240, Lausanne, Oct. 8-9, 2003. EPFL.

[24] V. Berrutto and M. Fontoynont. Applications of CCD cameras to lighting research: Review and extension to the measurement of glare indices. In *Proceedings CIE 119, 23rd Session*, pages 192–195, New Delhi, 1995.

[25] T. Kondo, T. Iwata, and K.-I. Kimura. Study on the evaluation system of visual environment including daylight. In *Proceedings Right Light 4, Vol. 2*, pages 129–136, Copenhagen, Denmark, 1997. IAEEL.

[26] L. Michel, D. Francioli, and J.-J. Meyer. Digital image facilities for visual comfort evaluation. In *Proceedings Solar Energy in Buildings CISBAT*

2001, pages 205–210, Lausanne, Oct. 3-4, 2001. EPFL.

[27] D. Francioli and J.-J. Meyer. Etude de l'éblouissement au moyen d'un photoluminancemètre numérique. In *Proceedings CISBAT 2003*, pages 265–270, Lausanne, Oct. 8-9, 2003. EPFL.

[28] G.J. Ward. Measuring and modeling anisotropic reflection. *ACM SIGGRAPH Computer Graphics*, 26(2):265–272, July 1992.

[29] J.-M. Deniel. *Modélisation des luminaires et des BRDF: réalisation, mesure et compression.* PhD thesis, Université de Rennes 1, Rennes, April 2002.

[30] M. Andersen, L. Michel, C. Roecker, and J.-L. Scartezzini. Experimental assessment of bi-directional transmission distribution functions using digital imaging techniques. *Energy and Buildings*, 33(5):417–431, May 2001.

[31] M. Andersen, M. Rubin, and J.-L. Scartezzini. Comparison between ray-tracing simulations and bi-directional transmission measurements on prismatic glazing. *Solar Energy*, 74(2):157–173, February 2003.

[32] M. Andersen, M. Rubin, R. Powles, and J.-L. Scartezzini. Bi-directional transmission properties of venetian blinds: Experimental assessment compared to ray-tracing calculations. *Solar Energy*, In Press.

[33] M. Andersen. Light distribution through advanced fenestration systems. *Building Research and Information*, 30(4):264–281, July 2002.

[34] M. Andersen. Matrix-based analysis of digital images: application to photogoniometric measurements with variable referential. *Optics and Lasers in Engineering*, In Press. Special issue "Optics in Switzerland".

[35] M. Andersen. *Innovative bidirectional video-goniophotometer for advanced fenestration systems.* PhD thesis, EPFL, Lausanne, 2004.

[36] M. Andersen. Dispositif de mesure de la distribution de luminance du

ciel basé sur des techniques d'imagerie numérique : développement et validation expérimentale. Master's thesis, EPFL, Lausanne, February 1998. Published under author's maiden name (Thys).

[37] R. Ramanath. Interpolation methods for the bayer color array. Master's thesis, North Carolina State University, Raleigh, NC, 2000.

[38] J. Breitenbach and J.L.J. Rosenfeld. Goniospectrometer measurements of the optical performance of a holographic optical element. *Solar Energy*, 68(5):427–437, 2000.

[39] E. Hecht. *Optics*, chapter 8. Addison-Wesley Publishing Company, Inc., USA, second edition, 1987.

[40] Commission Internationale de l'Eclairage. Practical methods for the measurement of reflectance and transmittance. *CIE*, 130, 1998.

List of Figures

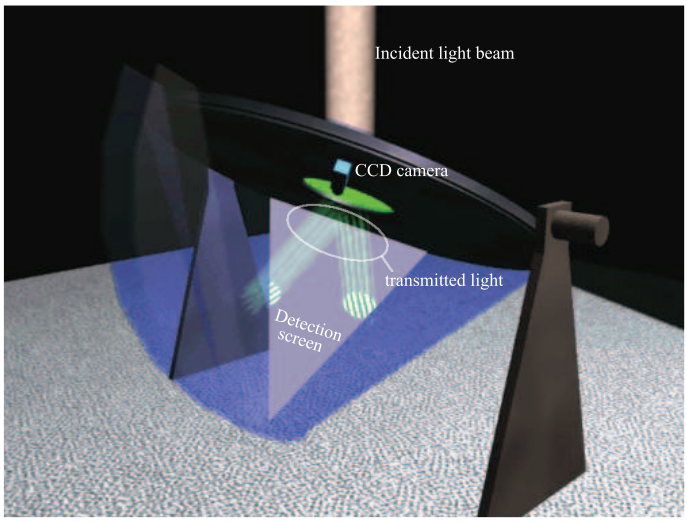

Fig. 1. Detection of the transmitted light flux for the LESO-PB / EPFL video-goniophotometer.

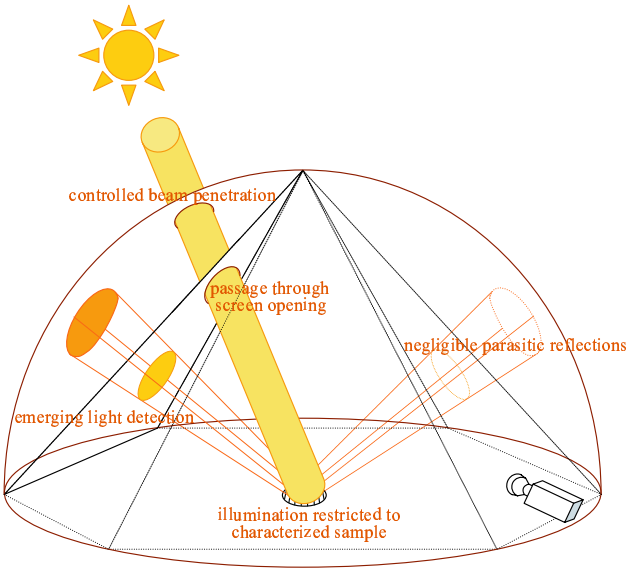

Fig. 2. Schematic representation of the constraints imposed for bidirectional reflection measurements.

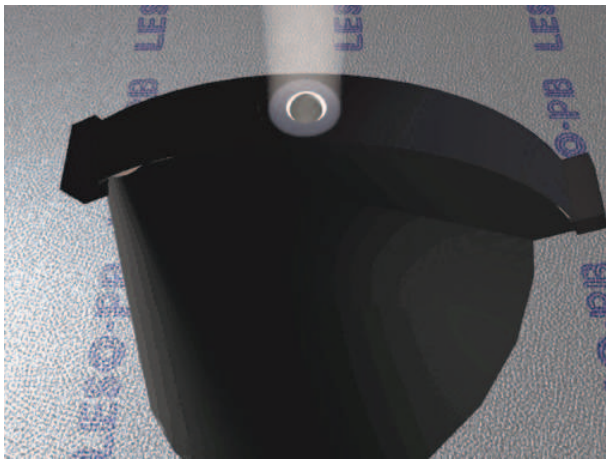

(a) Mobile strip hole over adequate elliptic opening

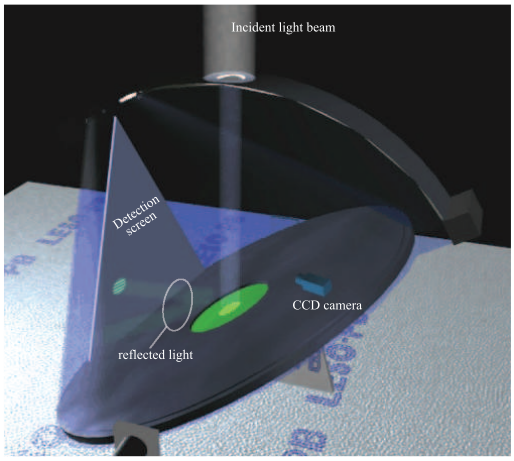

(b) Controlled illumination of sample surface

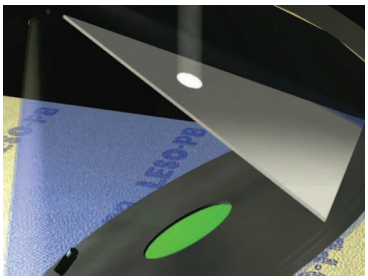

(c) Obstruction by screen

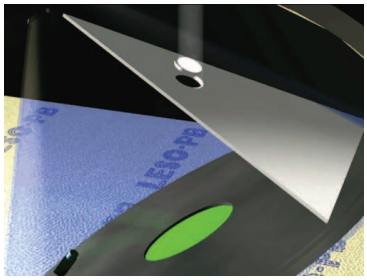

(d) Lifting of screen cover

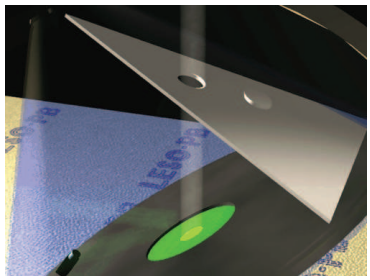

(e) Removal from beam path

Fig. 3. Control of incident beam penetration and path through obstructing screen.

(a) "Korrigan" followspot

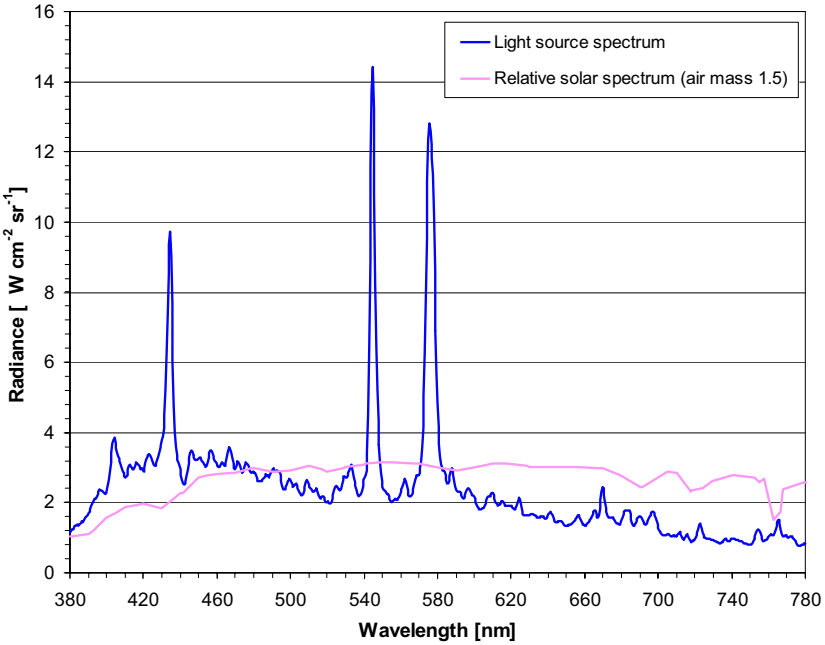

(b) Spectral characteristics and comparison to the solar spectral distribution (air mass 1.5, divided by a factor $3.5 \cdot 10^5$ for better display)

Fig. 4. Light source HMI 1.2 kW chosen for the BT&RDF goniophotometer.

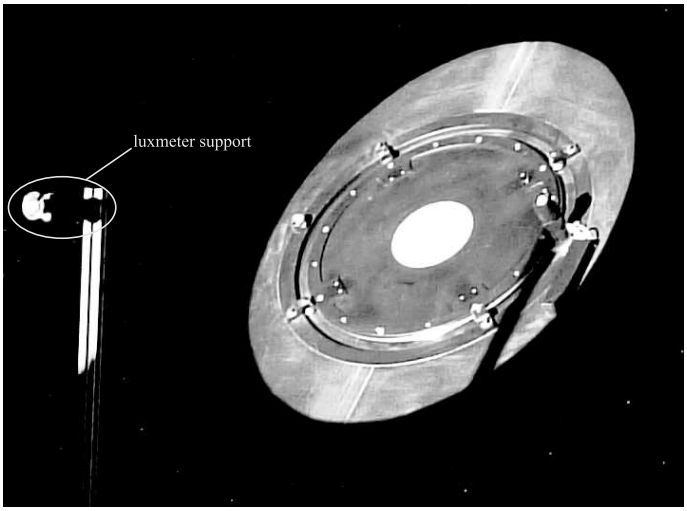

Fig. 5. Independent luxmeter support for simultaneous illuminance measurement.

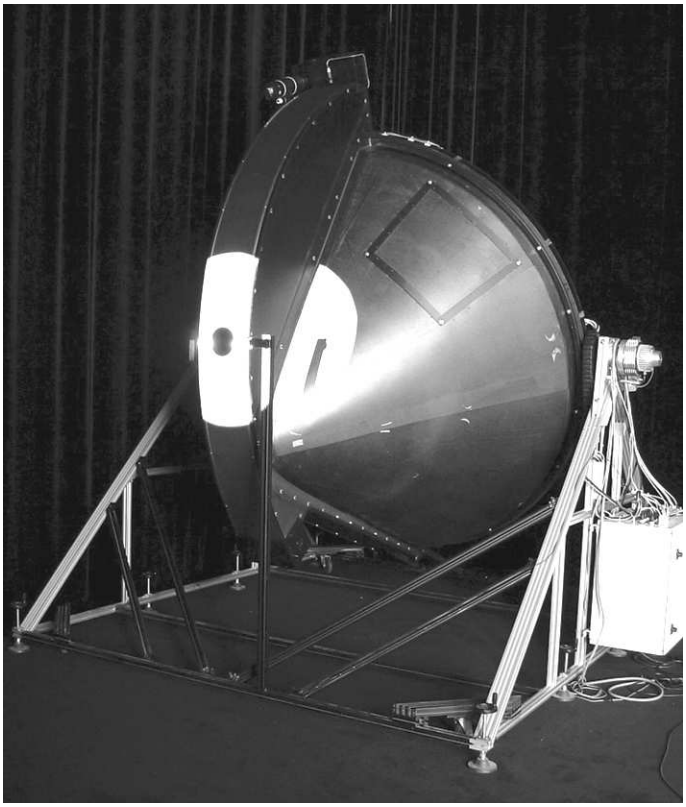

(a) Goniophotometer in reflection mode

(b) Metal sheet with cut-out ellipses

Fig. 6. Structural components of the BT&RDF goniophotometer.

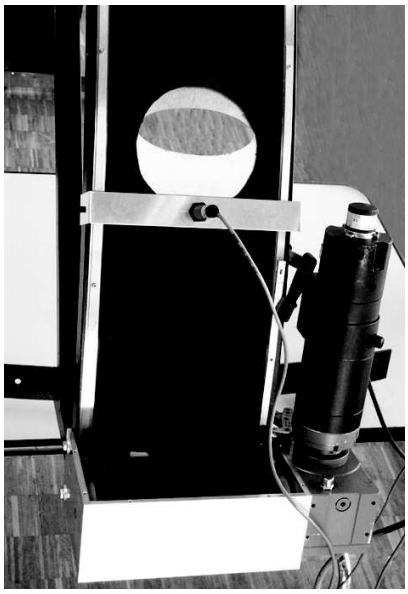

(a) Motorized strip winding with opto-sensor for home positioning

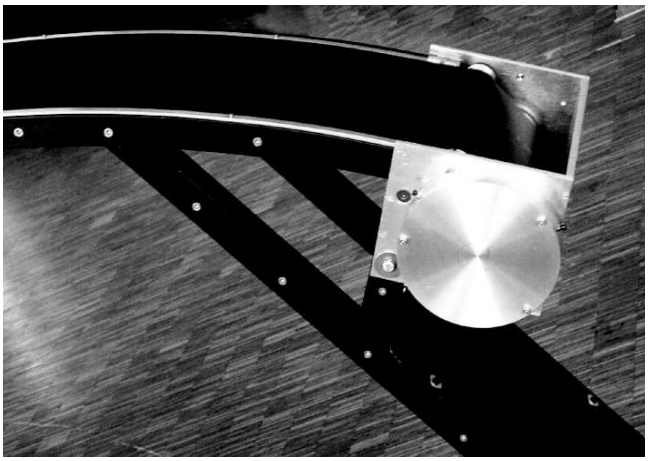

(b) Spring system to ensure strip tension

Fig. 7. Motorized unrolling of the synthetic strip for its adequate positioning on the metal sheet.

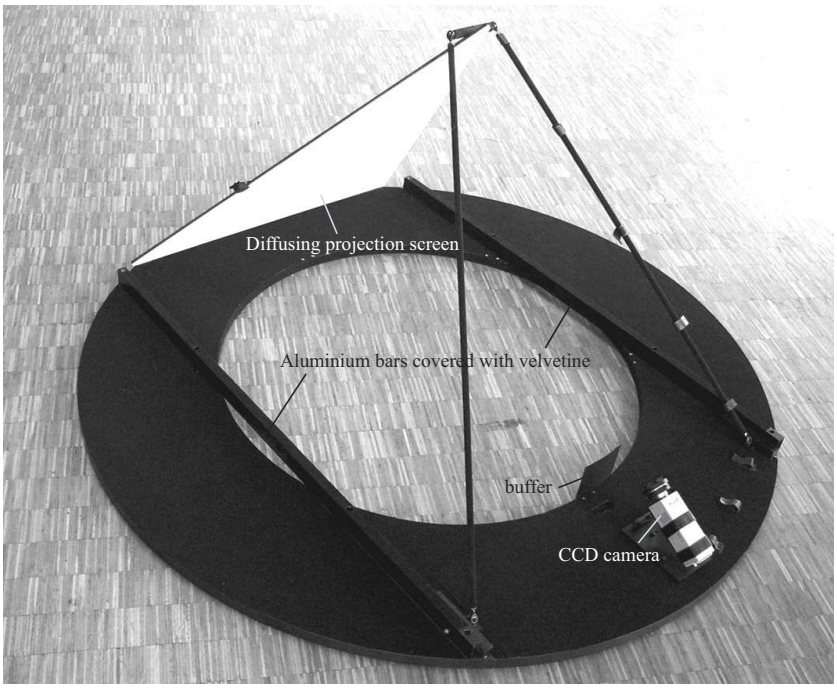

Fig. 8. Screen and camera facing each other on the rotating ring.

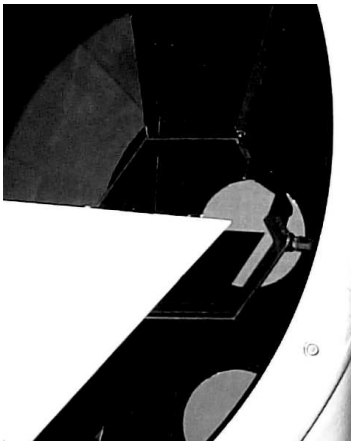

(a) Screen fixing system

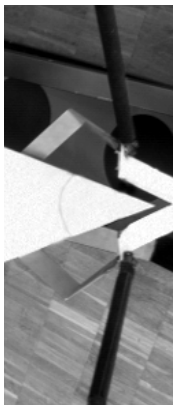

(b) Camera's view

Fig. 9. Hexagonal screen fixing piece to ensure incident beam path, with added apex to avoid screen image obstruction.

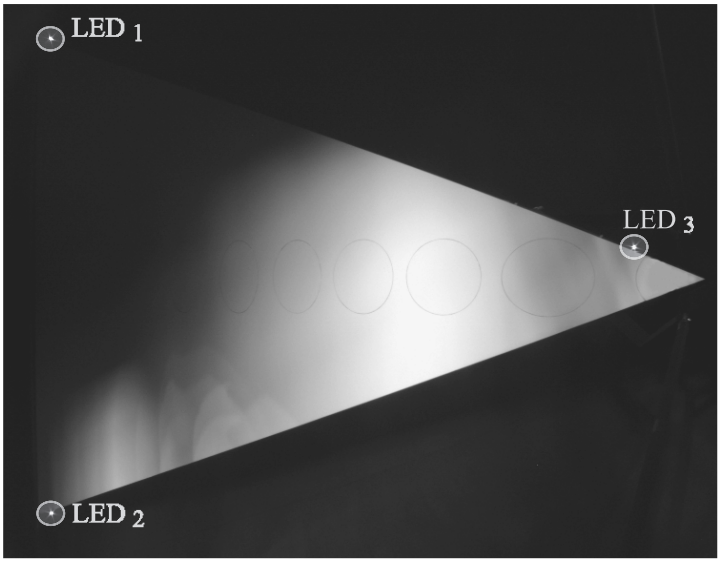

Fig. 10. Adjustment of the image pixels corresponding to the screen detection area thanks to three LED's localized on the image.

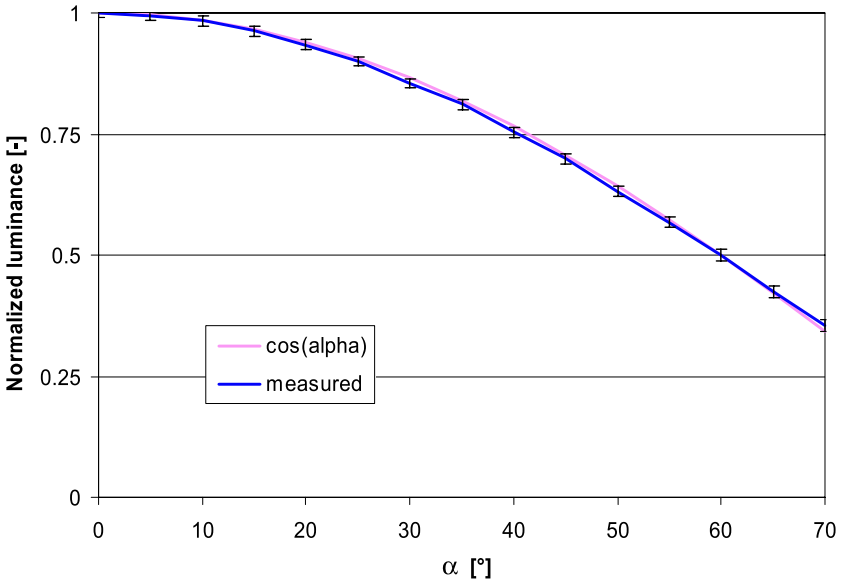

Fig. 11. Luminance on the screen surface as a function of impinging angle α compared to the expected $\cos\alpha$ law.

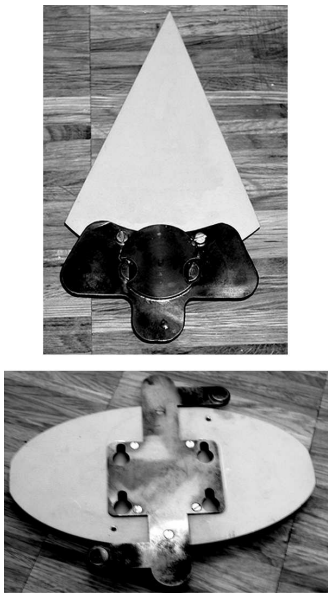

(a) Screen covers

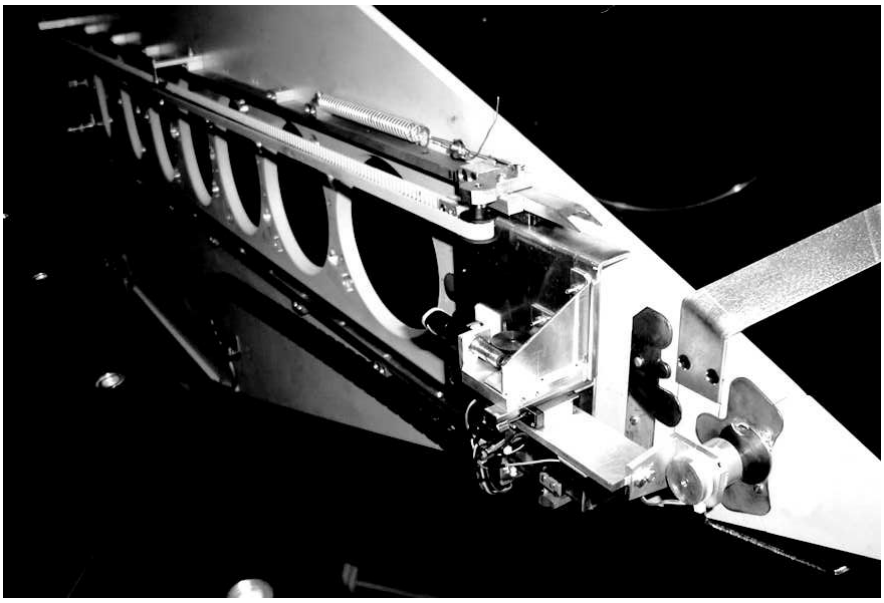

(b) Wagon and steering rails

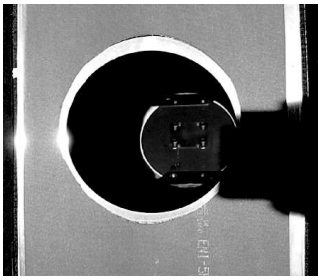

(c) Obstructing cover

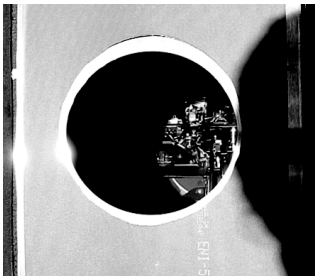

(d) Extraction

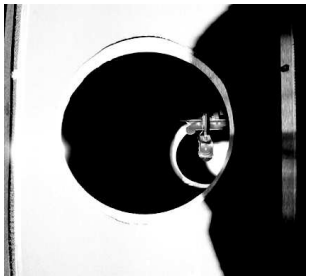

(e) Removal

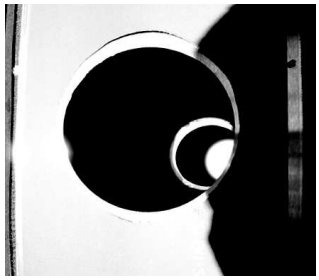

(f) Illumination

Fig. 12. Motorized screen with removable covers for incident beam path.

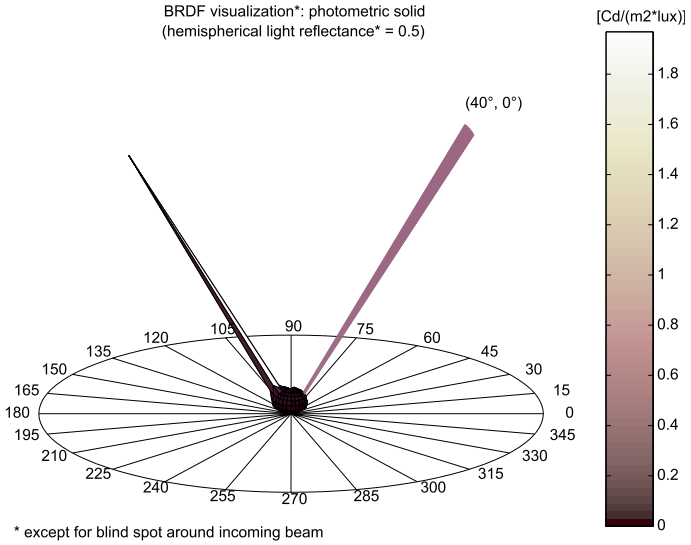

(a) Opalescent plexiglas, $(\theta_1, \phi_1) = (40°, 0°)$

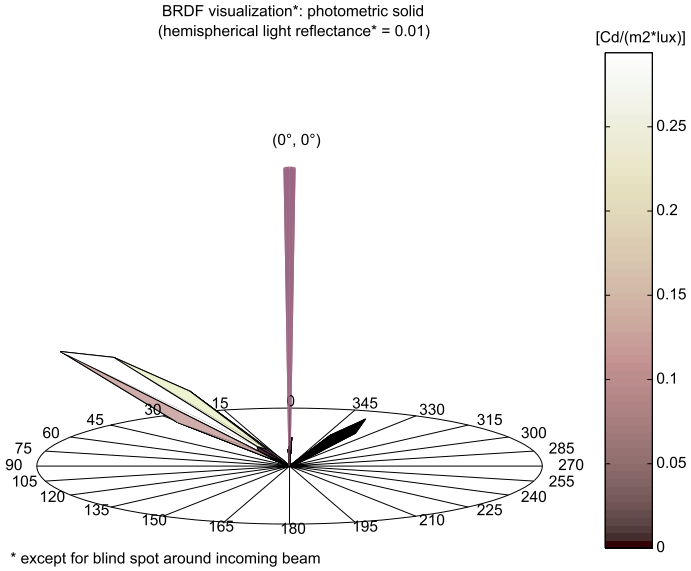

(b) Holographic film (HOE), $(\theta_1, \phi_1) = (0°, 0°)$

Fig. 13. BRDF representation as a photometric solid.